SOUND SOURCE DETECTION FROM RAW WAVEFORMS WITH MULTI-SCALE SYNPERIODIC FILTERBANKS

Anonymous authors
Paper under double-blind review

ABSTRACT

Accurately estimating sound sources' temporal location, spatial location and semantic identity label from multi-channel sound raw waveforms is crucial for an agent to understand the 3D environment acoustically. Multiple sounds form a complex waveform mixture in time, frequency and space, so accurately detecting them requires a representation that can achieve high resolutions across all these dimensions. Existing methods fail to do so because they either extract hand-engineered features (*i.e.* STFT, LogMel) that require a great deal of parameter tuning work (*i.e.* filter length, window size), or propose to learn a single filter bank to process sound waveforms in a single-scale that often leads to a limited time-frequency resolution capability. In this paper, we tackle this issue by proposing to learn a group of parameterized synperiodic filter banks. Each synperiodic filter's length and frequency response are inversely related, hence is capable of maintaining a better time-frequency resolution trade-off. By alternating the periodicity term, we can easily obtain a group of synperiodic filter banks, where each bank differs in its temporal length. Convolution of the proposed filterbanks with the raw waveform helps to achieve multi-scale perception in the time domain. Moreover, applying synperiodic filter bank to recursively process a downsampled waveform enables us to also achieve multi-scale perception in the frequency domain. Benefiting from the advantage of the multi-scale perception in both time and frequency domain, our proposed synperiodic filter bank groups learn a data-dependent time-frequency resolution map. Following the learnable synperiodic filter bank group front-end, we add a Transformer-like backbone with two parallel soft-stitched branches to learn semantic identity label and spatial location representation semi-independently. Experiments on both direction of arrival estimation task and the physical location estimation task shows our framework outperforms existing methods by a large margin. Replacing existing methods' front-end with synperiodic filter bank also helps to improve the performance.

1 INTRODUCTION

The fundamental task for an agent to perceive and interact with the 3D environment is to know the location and semantic identity of its nearby objects. The location includes spatial location that is either stationary or moving, temporal location like start time and end time. Vision-based such environment perception has received large attention in the past decade and we have witnessed huge progress in tasks such as object detection(Liu et al., 2016; Lin et al., 2014; Yang et al., 2019), classification(He et al., 2016a) and tracking(Wang et al., 2019). Nevertheless, the sound-based counterpart research has far lagged behind, despite all the fascinating properties sound signal exhibits. For example, sound is ubiquitous and insensitive to ambient illumination change, it has no field-of-view (FoV) constraints and is capable of circumventing physical barriers to perceive scene beyond line-of-sight. As a complementary sensing approach to vision, sound-based environment perception is of vital importance for acoustic scene understanding. A typical example is the sound source detection (answer where is it, when does it happen and what is it), given the recorded multi-channel sound waveforms.

To detect sound sources, we often deploy a spatially-configured microphone array to record an acoustic environment. Unlike camera or LiDAR scanner that directly captures RGB image or measures the range distance, sound waveform itself is a highly compressed one-dimensional points with high sampling rate, all sound source signals are compressed and mixed into the one-dimensional

data format. Since different sound sources have different frequency property, it is essential convert waveform into time-frequency representation so that frequencies hidden in the waveform are explicitly split out. This is often achieved by projecting the raw waveform into various orthogonal frequency basis. At the same time, a sound source's spatial location clue lies in inter-channel difference of recorded waveforms (*i.e.* phase difference in this work). It is essential to design a neural network that jointly encodes mono-channel time-frequency representation and inter-channel phase difference from the raw waveforms in a unified, parameter-frugal and computation-efficient manner. The learned representation should have elegant resolution in both time, frequency and space domain so that sound sources can be precisely detected.

However, learning such representation is a tough task. Challenges derive from both theoretical side and practical side. According to Uncertainty Principle, we cannot achieve the optimal resolution in time and frequency domain at the same time, but instead keep a trade-off between them. For example, shorter filters are often preferred to achieve high time resolution, but longer filters are required to achieve high frequency resolution, especially for low-frequency sound signal. Traditional hand-engineered sound feature(Davis & Mermelstein, 1980; Cao et al., 2021; Tho Nguyen et al., 2020; Brandstein & Silverman, 1997) and some recently proposed learnable filter bank(Ravanelli & Bengio, 2018; Zeghidour et al., 2018) empirically set the same length for all filters, resulting in human-biased, unadjustable time-frequency resolution map. Some other work(Zeghidour et al., 2021) correlates filter frequency response and filter length by initializing in mel-scale, but it is not scalable nor stable because the final initialization depends on the filter number. Moreover, all existing methods process raw waveform with one-scale filter bank, we argue that the one-scale sound perception easily leads to incomprehensive sound sources sensing, especially when sound sources have different frequency property or undergo various spatial motion.

In this paper, we first give comprehensive theoretical analysis on the filter bank impact on its extracted feature's time and frequency resolution. Based on the analysis, we propose a simple yet effective synperiodic filter bank construction strategy in which each filter's frequency response and length are correlated by rotating periodicity such that each filter's length is inversely proportional to its frequency response. The synperiodic filter bank thus internally maintains a better time-frequency resolution trade-off than traditional fixed-length filter bank. Coupling the filter length with its frequency response helps us to reduce human intervention in filter bank design. By simply alternating the periodicity term, we further construct a group of synperiodic filter banks, with which we achieve multi-scale perception in time domain. At the same time, by applying a synperiodic filter bank to process one raw waveform as well as its consecutively-downsampled versions, we achieve multi-scale perception in frequency domain. The multi-scale perception in both time and frequency domain of synperiodic filter bank enables the neural network to dynamically learn better representation for sound source detection in a data-driven way. It is worth noting that synperiodic filter bank parameter number is just linear to filter number (adds up to less than 1% of the whole parameter number) and it can be efficiently implemented as a 1D convolution operator.

Following the aforementioned learnable front-end, we add a Transformer-like backbone network with two paralleling branches with intermediate soft-parameter sharing to learn sound source's semantic and spatial location related representation both jointly and separately. Experiment on both direction-of-arrival (DoA) task and physical location estimation task shows that our proposed framework outperform comparing methods by a large margin. Replacing existing method's head with our proposed synperiodic filter bank also improvdes the performance.

2 Related Work

Sound signal processing has been thoroughly studied in traditional digital signal processing area. The preliminary step of sound signal processing is usually to convert raw waveform into 2D time-frequency representation, and the fundamental idea is to project the raw waveform into orthogonal basis of different frequencies. There are two main realms: Fourier transform based and Wavelet based transform(Sturm, 2007). Traditional sound features are human-auditory system biased. For example, they often convert frequency bins into mel-scale to imitate human hearing system like MFCC(Davis & Mermelstein, 1980), LogMel(Cao et al., 2021; Grondin et al., 2019), the filter length is empirically chosen and often a windowing is added to avoid spectrum leakage. For inter-channel phase difference encoding, it is often recommended to encode in frequency domain due to the less-computation

advantage. Typical phase difference features include GCC-Phat(Brandstein & Silverman, 1997) and intensity vector(Cao et al., 2021).

Sound source detection has been previously treated as sound structure(Thrun, 2006), sound object(He et al., 2021) and sound event detection and localization (SELD task)(Adavanne et al., 2018; Thi Ngoc et al., 2021). It involves jointly identifying a sound source's semantic label and predicting its spatial location, the two sub-tasks have been thoroughly studied separately in acoustics(Nandwana & Hasan, 2016; Mohan et al., 2008) and computer vision community(He et al., 2016a). Benefiting from the success of the traditional hand-engineered sound feature and the large availability of mature image-based deep neural networks(He et al., 2016a), most work(Grondin et al., 2019; Cao et al., 2021; Grondin et al., 2019; Adavanne et al., 2018; Thi Ngoc et al., 2021) tackle the task by first extracting hand-engineered sound feature and then feeding them to mature image-based neural networks. This workflow is straightforward and often guarantees reasonably good results but it is not end-to-end trainable and heavily depend on image side which may not be optimal for sound processing. At the same time, some work(He et al., 2021; Adavanne et al., 2018; Tho Nguyen et al., 2020) have simplified the problem by assuming no two sound sources of the same semantic label but different spatial location happen at the same time. This assumption avoids semantic label and spatial location association issue but the simplified case may not reflect real scenarios.

In recent years, a bunch of work tried to design neural work to directly learn from raw sound waveform, ranging from the earlier methods that directly apply stacked layers to process raw waveform(Schneider et al., 2019; Palaz et al., 2013; Jaitly & Hinton, 2011; Sainath et al., 2013) to the recent frequency-sensitive filter bank learning methods(Zeghidour et al., 2021; Ravanelli & Bengio, 2018; Zeghidour et al., 2018; He et al., 2021; Hoshen et al., 2015; Sainath et al., 2015; Luo & Mesgarani, 2019). The filter bank parameter is initialized in either mel-scale(Ravanelli & Bengio, 2018; Zeghidour et al., 2021; He et al., 2021; Zeghidour et al., 2018) or as Gammatone filter(Hoshen et al., 2015; Sainath et al., 2015). SoundDet(He et al., 2021) is the first work to directly learn from multi-channel raw waveforms to detect sound sources. It designs MaxCorr filter bank to directly convolve with multi-channel raw waveforms to learn phase difference aware features.

Multi-scale representation has a rich history in computer vision community ((Liu et al., 2016; 2021; Lin et al., 2016; He et al., 2016b)), in which multi-scale representation strategy has been proposed to accommodate large object scale variation. For example, Single Shot MultiBox Detector(Liu et al., 2016) combines feature maps of various scale to cover potential objects of sizes. In addition to spatial multi-scale representation, feature space multi-scale representation has been explored as well. For example, He *et. al.*(He et al., 2016b) incorporate features arising from intermediate layers to boost attribute recognition. In sound signal processing, Stéphane Mallat(Bruna & Mallat, 2013; Mallat, 2012) proposed wavelet scattering to obtain multi-scale sound representation by iteratively treating the proceeding processed sound waveform as new virtual waveform for further process.

3 Sound Source Detection from Multi-Channel Raw Waveforms

3.1 Sound Source Detection Problem Definition

We use a spatially-deployed microphone array, like four closely-bounded microphones in a circular coplanar configuration, to record an acoustic environment where various sound sources undergo independent and unconstrained spatial motion. Recorded multi-channel raw waveforms are represented as $W = \{x_i(t)\}_{i=1}^{4}$, each waveform is one-dimensional vector of size T sampled at a fixed sampling rate. We denote K sound sources involved in the waveforms by $S = \{s_k = (t_s^k, t_e^k, sp_k, sl_k)\}_{k=1}^{K}$, one single sound source corresponds to a start time t_s, end time t_e, stationary or moving spatial motion sp and a semantic identity label sl. Our goal is to learn a representation $\boldsymbol{\mathcal{P}}$ that is representative enough to detect sound sources both temporally, spatially and semantically. $\boldsymbol{\mathcal{P}}$ is a temporal framewise representation of shape $T_1 \times N$. We propose to learn $\boldsymbol{\mathcal{P}}$ directly from the raw waveforms via a deep neural network $\boldsymbol{\mathcal{F}}$ parameterized by θ,

$$\boldsymbol{\mathcal{P}}_{T_1 \times N} = \boldsymbol{\mathcal{F}}(W_{T \times 4}|\theta), \quad T_1 \ll T \tag{1}$$

A learned elegant representation should have large resolution in both time, frequency and space domain and exhibit strong capability at addressing three intrinsic challenges: Polyphonicity, sound

sources are mutually independent, they can freely overlap temporally; Time-scale variance, the temporal duration of different sound sources varies enormously, from seconds to minutes long; Datasize, sound waveform is sampled with large sampling rate, resulting in large data size.

3.2 Sound Source Clue from Sound Raw Waveforms

Sound source presence lies in the time-frequency representation. To obtain such time-frequency representation $X(w, \hat{t})$ for a mono-channel waveform $x(t)(\hat{t} \ll t)$, short-time Fourier transform (STFT) is often utilized to project it onto Fourier orthogonal basis $\{e^{iwt}\}_{w \in \mathbb{Z}}$. In practice, the raw waveform is first segmented into $\hat{t}$ overlapping short segments, the k-th column of $X(w, \hat{t_k})$ corresponds to the transform result on the k-th segment waveform $x(t)_k$. To prevent spectral leakage, a windowing function $w(\cdot)$ (*i.e.* Hanning window) is often added.

$$X(w, \hat{t_k}) = \sum_{t=1}^{m} x(t)_k \cdot (e^{i \cdot wt} \cdot w(t)) \tag{2}$$

where i is the imaginary unit. m is the waveform segment length. Sound source' spatial location mainly derives from the inter-channel interaction among recorded multi-channel waveforms. One typical interaction is the signal time delay of arrival or phase-difference between any two microphones. For two channel waveforms $x_1(t)$ and $x_2(t)$, their interaction in time domain can be represented as,

$$x_2(t) = x_1(t - t_0) + n(t) \tag{3}$$

where t_0 is the phase-difference and $n(t)$ is an additive noise term. Computing t_0 in time domain is computation-costly. A more desirable way is to instead compute in frequency domain, like traditional GCC-Phat(Brandstein & Silverman, 1997) and intensity vector do. Specifically, the Eqn.(3) can be represented in frequency domain as,

$$X_2(w) = X_1(w) \cdot e^{-i \cdot wt_0} + N(w) \tag{4}$$

Based on Eqn.(4), we further compute cross-spectrum $X_2(w) \cdot X_1^*(w)$ to explicit encode phase-difference. Here $X_1^*(w)$ is the conjugate of $X_1(w)$. In this paper, we choose to encode the spatial location relevant feature in frequency domain because it benefits us to align sound source's time-frequency feature extraction and spatial location feature extraction together, and we jointly learn them with the same filter bank in a unified way. More details is given in the Appendix A.1.

3.3 Multi-Scale Synperiodic Filter Bank

We denote the general filter bank of M filters by $\mathcal{F} = \{\mathcal{F}_i(w_i, \sigma_i, l_i) = \phi(w_i) \cdot \omega(\sigma_i)\}_{i=1}^{M}$. Each single filter $\mathcal{F}_i$ is created by multiplying the frequency-selective filter $\phi(w_i)$ of frequency response w_i (*i.e.* sinusoidal basis or band-pass basis(Ravanelli & Bengio, 2018)) with a windowing function $\omega(\sigma)$. The windowing function has locality property which means it is just active within a local region controlled by σ (*i.e.* Gaussian kernel window). Then l_i points are cropped around the active region and treated as a frequency-selective filter (usually $l_i > \sigma_i$). Existing filter bank differs in their way of parameter setting, including filters' frequency response distribution, filter length length and windowing function. In classic hand-engineered features such as short-time Fourier transform (STFT) and LogMel feature, all these parameters are empirically chosen. Contrary to STFT, wavelet transform(Sturm, 2007) inversely correlates window length with frequency response so that the active region of the filter is internally decided by its frequency response.

Time-Frequency Dynamic Resolution The frequency resolution indicates the ability of discerning two adjacent frequency bins in frequency domain, while similarly time resolution corresponds to the capability of precisely localizing a sound object in time domain. The resolution in time and frequency domain jointly influence spatial localization precision because we encode spatial location related feature on pre-extracted time-frequency feature (see Eqn.(4)). According to Uncertainty Principle, however, the frequency resolution Δ_f and time resolution Δ_t satisfies $\Delta_f \cdot \Delta_t \geqslant C$ (C is a constant). It means we cannot get optimal resolution in both time and frequency domain at the same time, but

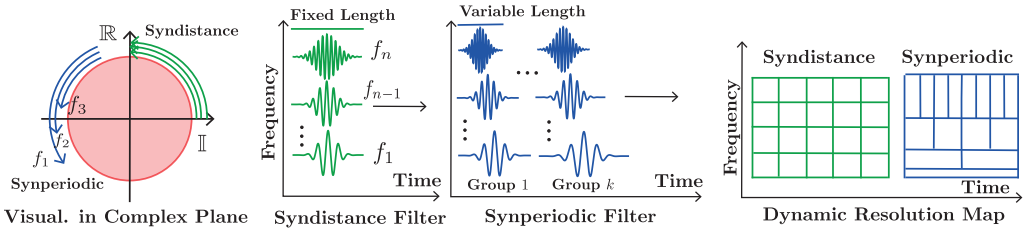

Figure 1: Synperiodic filter bank illustration: Syndistance filter bank (green color) rotates the same distance in complex plane and thus has the same kernel length, regardless of frequency it carries. Its time-frequency dynamic resolution map is thus rectangular. our proposed synperiodic filter bank (blue color) are generated by rotating the same periodicity number. So filter carrying lower frequency has larger kernel size than those with higher frequency response. As a result, synperiodic filter bank's time-frequency dynamic resolution map that is able to achieve a better trade-off than traditional syndistance filter bank.

rather keep a trade-off between them: increasing the resolution in one domain inevitably sacrifices the resolution in the other domain.

Traditional hand-engineered sound feature's time-frequency resolution map is fixed because all filter bank construction relevant parameters are empirically chosen. Therefore, its time-frequency resolution map is evenly divided across both the time and frequency domain (see Fig.1 second last figure). Relaxing the frequency response and windowing length as trainable(Zeghidour et al., 2021) helps to achieve a better time-frequency resolution trade-off. The improvement is, however, limited because it uses one filter bank of the same filter length to process all sound signals (or perceive at one-scale). We categorize these traditional filter bank as syndistance filter bank to emphasize their equal temporal length property across all frequency responses.

In this paper, we rethink filter bank design and propose a synperiodic filter bank construction strategy, and further achieve multi-scale processing in both time and frequency domain. Our motivation is based on the fact that high frequency sound signal can be adequately detected with a shorter filter, enlarging the filter length doesn't necessarily increase the frequency resolution but inevitably reduces the filter's time resolution. Conversely, lower frequency sound signals require wider filters. It thus shows using the same window size for all filters across the frequency range is not a good choice, a more desirable way is to use narrower filters for filters with higher frequency responses. With this guide in mind, we propose a synperiodic filter bank construction strategy. To better understand the main difference between syndistance filter bank and our proposed synperiodic filter bank, we can visualize them in complex-valued plane (see Fig.1, left-most one), in which a filter is a complex exponential rotating in the complex plane counter-clockwisely, the rotating speed corresponds to the frequency response it carries. In the complex-valued plane, all syndistance filters rotate to the same distance. Synnperiodic filters, however, rotate to a predefined periodicity ρ, naturally resulting in narrow window for high-frequency filters and wide window for low-frequency filters.

Synperiodic filter bank lends us three advantages: it first avoids us setting window length for each filter separately, which is quite empirical and random; second, the constructed filter bank naturally maintains a good time-frequency resolution trade-off by design; third, by simply varying the periodicity term ρ, we can easily obtain a group of synperiodic filter bank to process the raw waveform in multi-scale manner (as we will present in below). Our synperiodic filter bank construction strategy shares similar idea with Wavelet transform(Sturm (2007)) where it uses a Gaussian kernel to squeeze or expand a sinusoidal basis wave to generate narrow-window-high-frequency and wide-window-low-frequency filter bank. The difference is that we don't have explicitly set the "squeezing rate" for each filter separately and synperiodic filter bank is learnable. Specifically, our proposed synperiodic filter bank can be represented as,

$$\mathcal{F}^{\rho}_{synperiodic} = \{f_i(w_i, \rho, l_i) = \phi(w_i) \cdot \omega(w_i, \rho)\}_{i=1}^{M} \tag{5}$$

where we can see that the windowing function just depends on the center frequency w_i and the periodicity term ρ. By varying the periodicity term ρ, we can obtain a group of synperiodic filter

banks $\mathcal{F}_{synperiodic} = \{\mathcal{F}^{\rho_1}, \mathcal{F}^{\rho_2}, \cdots, \mathcal{F}^{\rho_n}\}$. The comparison between syndistance filter bank and synperiodic filter bank is shown in Fig. 1.

There are many $\omega(w_i, \rho)$ choices, as long as we guarantee the window length gradually reduces as the the frequency response increases. The simplest choice is to treat $\omega(w_i, \rho)$ as a constant, but we find it either results in too wide window for low-frequency filters too narrow window for high-frequency filters. To mitigate this dilemma, we use logarithmic windowing function $\omega(w_i, \rho) = 27 \cdot \log_{10}(w_i) - \rho$. We choose the ρ as $[-6, -11, -16]$ respectively to alternate the periodicity term to construct the three synperiodic filter bank groups. The design of this window function is motivated by the mel-scale frequency initialization strategy, in which two neighboring frequencies are more closely spaced in lower frequency part and higher frequency part. By roughly setting a filter's band width to be equal to the distance between its preceding and next neighboring frequency location in frequency domain, converting to time domain we can roughly get a logarithmic scale frequency-periodicity relationship (see Fig.4 in Appendix). In our implementation, synperiodic filter is created by multiplying a sinusoidal filter with learnable frequency response initialized in mel-scale by a Gaussian window with learnable width initialized through the windowing function. Please note that each synperiodic filter bank group is initialized with independent learnable frequencies and window length, they are independently updated during training.

3.4 Multi-Scale Learning in Time and Frequency Domain

We use previously constructed synperiodic filter bank groups to convolve with mono-channel sound waveform with the same step size and padding strategy, resulting in the same size output for each single group. Since different filter group has window periodicity (ρ), we naturally achieve multi-scale learning in time domain. It maximally avoids us empirically selecting one window scale ρ which might not be a human-biased, but instead uses a group of filter bank to enforce the neural network to strike a better time-frequency resolution trade-off in a data-driven way.

We further propose a strategy to enable multi-scale learning in frequency domain. The strategy is hierarchical: given a raw sound waveform with sampling frequency F_S, synperiodic filter bank's frequency is initialized in the range $[0, \frac{F_S}{2}]$ under Nyquist sampling theorem. If we downsample the sound waveform by a factor of 2, the resulting waveform can be processed by the part of the of the original filter bank whose frequency response lies in $[0, \frac{F_S}{4}]$. We can thus reuse the lower-half filter bank to process the downsampled waveform. This process that 2x-downsampling the waveform to get a new waveform and further process the new waveform with the lower-half frequency filters in the current filter bank can potentially iterate a couple of times (in our case three times), resulting in a hierarchical and multi-scale convolution structure in frequency domain. The multi-scale frequency learning strategy is illustrated in Fig. 2. Multi-scale learning in frequency domain brings us two extra benefits: from data augmentation perspective, hierarchical 2x downsampling the raw waveform naturally generated more waveform data, which helps a lot especially when labelling audio data is technically hard and time-consuming. From the causality perspective, the adjacent interval subsampling strategy leads to dilated convolution for lower-frequency filters because applying a filter to convolve with a downsampled waveform equals to convolve with the original waveform with dilated convolution (skip-2 connection). The skipped wider field of view (FoV) for lower frequency filters enables to learn better sound causality along the time axis (see Appendix A.4). In sum, by using learnable synperiodic filter bank groups to process the raw waveform in multi-scale manner, we can achieve a dynamic time-frequency resolution map that naturally maintains a better time-frequency resolution trade-off and is adjustable w.r.t. the the sound scene in a data-driven way.

Computational Analysis Synperiodic filter bank groups introduces minimal parameters (less than 1%) because they are parameterized filters. The parameter number is just linear to filter number. Their convolution with raw waveforms can also be efficiently implemented by matrix parallelization.

3.5 Tansformer-like Backbone with Two Soft-Stitching Branches

The aforementioned synperiodic filter bank generates initial feature representation of shape $[T_0, N_0, C]$, where T_0 is much smaller than the T but is still larger than T_1. N_0 equals to the filter number (in this paper, we use 256), C is channel number. We stack the feature processed by each synperiodic filter bank to form the channel dimension. Jointly learning framewise sound source semantic label and spatial location representation is a multi-task problem(Kendall et al., 2018;

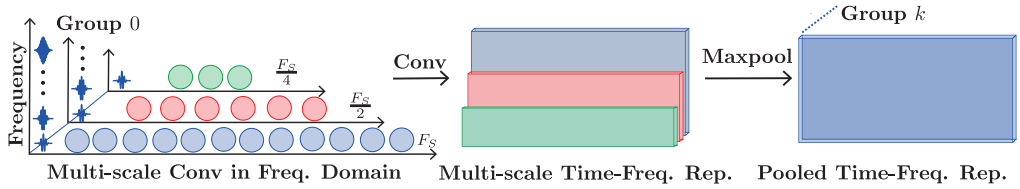

Figure 2: Multi-scale learning in frequency domain. Given the raw one channel sound waveform and pre-constructed synperiodic filter bank, we consecutively downsample the waveform by factor 2x, the newly downsampled waveform is processed by low-half filter bank from the proceeding filter bank. We can obtain time-frequency representation for on each frequency scale. These time-frequency representations share the same time length by adjusting step size. The final time-frequency representation is obtained by max-pooling them together.

Table 1: Evaluation result for DoA task. For Segment-based evaluation, we report detection error ER_{20°, F measure F_{20° under DoA threshold 20°, and classification dependent localization error LE_{CD} and localization recall LR_{CD}. For event-based evaluation, we report mAP/mAR. The "Input" column labels are: 0. Raw waveform, 1. Log-Mel, 2. GCC-Phat, 3. Intensity Vector.

Methods	Params	Input	Segment-Based Evaluation				Event-based Evaluation	
			$ER_{20^\circ}(\downarrow)$	$F_{20^\circ}(\uparrow)$	$LE(\downarrow)(^\circ)$	$LR(\uparrow)$	mAP(↑)	mAR(↑)
SELDNet(foa)(Adavanne et al., 2018)	0.5 M	1,3	0.63	0.46	23.1	0.69	0.087	0.152
SELDNet(mic)(Adavanne et al., 2018)	0.5 M	1,2	0.66	0.43	24.2	0.66	0.079	0.140
EIN(foa)(Cao et al., 2021)	26.0 M	1,2	0.30	0.77	8.9	0.84	0.134	0.256
SoundDet(foa)(He et al., 2021)	13.0 M	0	0.25	0.81	8.3	0.82	0.197	0.294
UTSC-Iflytek(foa+mic)(Wang et al., 2020)	Ensemble	1,2,3	0.20	0.85	6.0	0.89	-	-
SoundSynp(mic)	60.0 M	0	0.19	0.86	5.5	0.91	0.210	0.313
SoundSynp(foa)	60.0 M	0	**0.16**	**0.88**	**4.3**	**0.93**	**0.232**	**0.327**

Misra et al., 2016), and learning them in one neural network often leads to inferior performance. To mitigate this dilemma, we propose a Transformer-like backbone with two paralleling branches to learn each sub-task separately. To encourage information communication, we add a layerwise information exchange module. For any two intermediate semantic label feature f_s^i and spatial location aware feature f_g^i learned by the paralleling i-th network block, a learnable weight W_i is introduced to linearly combine them together to get an updated f_s^i and f_g^i before feeding them to the next layer, $[f_s^i, f_g^i] = W_i \cdot [f_s^i, f_g^i]$. In practice, the Transformer-like backbone gradually reduces the learned feature's temporal length but increase the feature length accordingly. Finally we can get the final sound source representation of shape $[T_1, N]$. On top of the representation, we add trackwise permutation-invariant training (PIT) strategy(Cao et al., 2021) to train the whole neural network in an end-to-end manner. The permutation invariant training strategy helps to address the polyphonicity challenge because it encapsulates a potential sound source's semantic label and spatial location in a track, so it won't be influenced by other sound sources.

4 Experiments

We conduct experiments on two tasks: direction of arrival (DoA) and physical location estimation. DoA estimation requires to decide arrival angle the sound source w.r.t. the microphone array. Physical location tends to directly localize a sound source's physical location (*i.e.* (x, y, z) coordinates). For DoA estimation task, we use DCASE2020 sound event detection and localization dataset(Politis et al., 2020). It contains 14 sound sources with azimuth range $[-180^\circ, 180^\circ]$ and elevation range $[-45^\circ, 45^\circ]$. Two recording formats are available: FOA and MIC-array (refer to Appendix for detailed discussion). For more details about this dataset, please refer to (Politis et al., 2020). For physical location estimation, we use pyroomacoustics(Scheibler et al., 2018) to simulate the dataset.

We adopt two metrics: segment-based and event-based metric. Segment-based metric is widely adopted evaluation metric(Adavanne et al., 2018; Cao et al., 2021) and it evaluates in segment-wise manner by coupling semantic label and spatial location prediction result: a semantic-correctly detected sound source needs to be spatially close enough to its ground truth location in order to be regarded as true positive. Event-based based metric is newly proposed by(He et al., 2021) to comprehensively evaluate under different confidence scores(Lin et al., 2014).

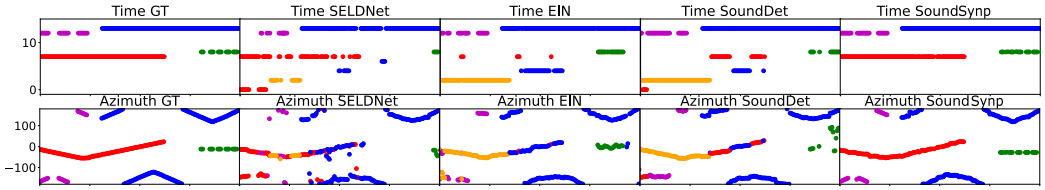

Figure 3: Qualitative comparison on DoA task. We show detected sound source temporal location (top row) and azimuth (bottom row). The horizontal axis is time, the vertical axis is semantic label (top) and azimuth in degree(bottom). Different color indicates different sound source category.

We call our framework SoundSynp and compare it with four main methods: SELDNet(Adavanne et al., 2018), EIN(Cao et al., 2021), SoundDet(He et al., 2021) and Utsc-Iflytek(Wang et al., 2020). SELDNet is the baseline model and it jointly trains sound source's semantic label and spatial location with a convolutional recurrent neural network (CRNN)(Chung et al., 2014). EIN(Cao et al., 2021) is a very recent work. It adopts multi-heads self-attention (MHSA)(Vaswani et al., 2017) to model temporal dependency and trackwise permutation-invariant training to the train the network. SoundDet(He et al., 2021) directly learns from raw waveform with MaxCorr kernels, followed by an encoder-decoder neural network and an object proposal generation head. Utsc-Iflytek(Wang et al., 2020) is ranked first in DECASE2020 challenge leaderboard[1], it combines MIC and FOA recording format and ensemble different models like ResNet(He et al., 2016a) and Xception(Chollet, 2017) together to infer the final prediction. Implementation detail is given in Appendix.

The result is given in Table1, from which we see that our proposed SoundSynp achieves the best performance over all other comparing methods by a large margin, under both segment-based and event-based evaluation metric. SELDNet, EIN and UTSC-Iflytek both use pre-extracted hand-engineered sound features, such as Logmel, GCC-Phat and Intensity Vector. SoundDet(He et al., 2021) and SoundSynp are the only two methods that directly learn from raw waveforms. At the same time, SoundSynp obtains better performance on FOA than MIC recording format, the same phenomena has been observed by all other methods. It thus shows FOA better fits for sound source detection than MIC. It is worth noting that Utsc-Iflytek(Wang et al., 2020) ensembles different powerful image-based 2D neural networks infer sound sources. However, our proposed SoundSynp still outperforms Utsc-Iflytek by a large margin. We don't report of mAP/mAR value of Utsc-Iflytek because it is a complex system and no detail about their system is available.

Ablation Study To further test effectiveness SoundSynp, we replace the hand-engineered sound feature of SELDNet, EIN and learnable MaxCorr filter bank of SoundDet with our Synperiodic filter bank to test the corresponding performance. It removes the influence of the backbone neural network of different models and thus helps us to get direct comparison of synperiodic filter bank with other front-end. Moreover, we modify SoundSynp to get different modified versions. (1) synperiodic filter bank with just multi-scale perception in frequency domain (SoundSynp_MSFreq), (2) just multi-scale perception in time domain (SoundSynp_MSTime), (3) Synperiodic filter bank with frequency responses linearly initialized in Nyquist frequency range (SoundSynp_Linear, compare with our mel-scale initialization), (4) just one synperiodic filter bank without multi-scale perception neither in time nor frequency domain (SoundSynp_SingleScale). (5) synperiodic filter bank with rectangular band-pass frequency response initialization (SoundSynp_Sinc), like SincNet(Ravanelli & Bengio, 2018) does. The detailed result is reported in Table 2, from which we can observe that: using synperiodic filter bank as a replacement of existing filter bank can help to improve the corresponding performance. The absence of multi-scale perception in either frequency domain or time domain inevitably reduces the performance. We find sound source semantic label detection suffers more in single-scale perception in time domain than in frequency domain (see better performance on ER_{20°, and F_{20° score), which shows frequency domain multi-scale perception is vital for semantic label estimation. Similarly, we can observe that multi-scale perception in time domain is vital for sound source spatial location estimation (see better performance on LE and LR score). Linearly initialized filter bank frequency response reduces the performance, which attests assign more filters to the lower frequency range is important. But this conclusion might be data-dependent because we find DCASE dataset contains many low-frequency sounds like burning fire and footsteps. Moreover, reducing the

[1]see this link for leaderboard report.

Table 2: Ablation study report. Internally, we replace SELDNet, EIN and SoundDet head with synperiodic filter bank (denoted as _Synp). Externally, we test different modified SoundSynp versions.

Methods	Blocks	Segment-Based Evaluation				Event-based Evaluation	
		$ER_{20^\circ}(\downarrow)$	$F_{20^\circ}(\uparrow)$	$LE(\downarrow)(^\circ)$	$LR(\uparrow)$	mAP(↑)	mAR(↑)
SELDNet(foa)(Adavanne et al., 2018)	Conv2D, biGRU	0.63	0.46	23.1	0.69	0.087	0.152
SELDNet_Synp(foa)(Adavanne et al., 2018)		0.57	0.49	22.1	0.75	0.093	0.165
SELDNet(mic)(Adavanne et al., 2018)	Conv2D, biGRU	0.66	0.43	24.2	0.66	0.079	0.140
SELDNet_Synp(mic)(Adavanne et al., 2018)		0.61	0.48	23.0	0.70	0.090	0.153
EIN(foa)(Cao et al., 2021)	Conv2D, MHSA	0.30	0.77	8.9	0.84	0.134	0.256
EIN_Synp(foa)(Cao et al., 2021)		0.27	0.79	8.3	0.87	0.138	0.258
SoundDet(foa)(He et al., 2021)	Conv1D, LSTM	0.25	0.81	8.3	0.82	0.197	0.294
SoundDet_Synp(foa) (He et al., 2021)		0.22	0.83	7.9	0.85	0.204	0.299
SoundSynp_MSFreq(foa)	Conv2D, MHSA	0.20	0.85	7.3	0.86	0.210	0.284
SoundSynp_MSTime(foa)		0.22	0.82	7.0	0.88	0.172	0.282
SoundSynp_Linear (foa)		0.21	0.83	8.8	0.83	0.168	0.259
SoundSynp_SingleScale(foa)		0.25	0.80	9.0	0.81	0.164	0.246
SoundSynp_Sinc(foa)		0.19	0.86	5.2	0.91	0.226	0.316
SoundSynp(foa)	Conv2D, MHSA	**0.16**	**0.88**	**4.3**	**0.93**	**0.232**	**0.327**

Table 3: Physical location estimation result report. We set distance threshold $1.0m$, which means a detected sound sources has to lie within this threshold in order to be treated true positive.

Methods	Segment-Based Evaluation				Event-based Evaluation	
	$ER_{1.0m}(\downarrow)$	$F_{1.0m}(\uparrow)$	$LE(\downarrow)(m)$	$LR(\uparrow)$	mAP(↑)	mAR(↑)
EIN(Cao et al., 2021)	0.45	0.71	0.71	0.73	0.114	0.240
EIN_Synp(Cao et al., 2021)	0.45	0.72	0.67	0.75	0.117	0.244
SoundDet(He et al., 2021)	0.43	0.67	0.68	0.74	0.118	0.271
SoundDet_Synp(He et al., 2021)	0.44	0.69	0.64	0.79	0.123	0.271
SoundSynp	**0.35**	**0.79**	**0.53**	**0.83**	**0.154**	**0.279**

synperiodic filter bank group to one groups with just single-scale perception leads to comparably the worst performance, it thus shows multi-scale perception in both time and frequency domain is essential for DoA-based sound source detection. Lastly, SoundSynp_Sinc leads to slightly inferior performance than our used mel-scale initialization strategy, it shows our proposed synperiodic filter bank is a general filter bank that can be adopted to other frequency sensitive filter bank.

One qualitative comparison is shown in Fig. 3. We can clearly see that SELDNet generates mixed prediction at different time steps and DoA locations. SoundDet and EIN give non-existing sound sources (orange color). When multiple sound sources happen at the same time (polyphonicity), SoundDet and EIN are easily failed to predict the right spatial location (discretized blue and red color). Our method predicts more spatially and temporally consistent sound sources by maximally keeping sound source's continuity and consistency.

Physical Location Estimation We use Pyroomacoustics simulator(Scheibler et al., 2018) to simulate a shoebox like room with $[7m, 5m, 3m]$ size. Four microphones (24kHz sampling rate) are configured in a plane with $5cm$ mutual distance and put in the room center ($[3.5m, 2.5m, 1.5m]$). We choose three commonly heard sounds from BBC sound effect site[2]: cat meowing, baby talking and dog barking. All these seed sounds last less than 10s. During simulation, we put all seed sound in the plane $z = 1.5m$ (we constrain to a plane because we find relaxing z easily leads EIN model to get stuck in a local minima like $[-1, -1, -1]$), but with x randomly in $[2m, 5m]$ and y randomly in $[1m, 4m]$, up to two sounds can happen at the same time. In sum, we have simulated 500 one-minute recordings (400 for train, 100 for test), with an average of four sounds recorded per recording. For physical location prediction, we regress the angle and range. The result is in Table 3. We do not report SELDNet result as we find it doesn't converge during train. We can see from the table that SoundSynp produces the best performance than over EIN and SoundDet network. Replacing their front-end with synperiodic filter bank also improves the performance. It thus shows our proposed SoundSynp is capable of learning representation for physical-location based sound source detection.

Discussion and Conclusion We have proposed a parameter-frugal and computation-efficient synperiodic filter bank, and further talked how to use it to achieve multi-scale perception in both time and frequency domain. Our proposed SoundSynp achieves state-of-the-art performance on sound source detection tasks. We believe synperiodic filter bank idea can be extended to process other acoustic data and tasks, which is also our next research direction.

[2]see https://sound-effects.bbcrewind.co.uk/

REFERENCES

Sharath Adavanne, Archontis Politis, Joonas Nikunen, and Tuomas Virtanen. Sound event localization and detection of overlapping sources using convolutional recurrent neural networks. In *IEEE Journal of Selected Topics in Signal Processing*, 2018.

M. S. Brandstein and H. F. Silverman. A robust method for speech signal time-delay estimation in reverberant rooms. In *IEEE International Conference on Acoustics, Speech, and Signal Processing (ICASSP)*, 1997.

J. Bruna and S. Mallat. Invariant scattering convolution networks. *IEEE Transactions on Pattern Analysis Machine Intelligence (TPAMI)*, 2013.

Yin Cao, Turab Iqbal, Qiuqiang Kong, Fengyan An, Wenwu Wang, and Mark D Plumbley. An improved event-independent network for polyphonic sound event localization and detection. In *IEEE International Conference on Acoustics, Speech, and Signal Processing (ICASSP)*, 2021.

François Chollet. Xception: Deep learning with depthwise separable convolutions. In *IEEE Conference on Computer Vision and Pattern Recognition (CVPR)*, 2017.

Junyoung Chung, Caglar Gulcehre, KyungHyun Cho, and Yoshua Bengio. Empirical evaluation of gated recurrent neural ntworks on sequence modelling. In *Adv. Neural Inform. Process. Syst.*, 2014.

Steven Davis and Paul Mermelstein. Comparison of parametric representations for monosyllabic word recognition in continuously spoken sentences. In *In IEEE Transactions on Acoustics, Speech, and Signal Processing*, 1980.

Francois Grondin, James Glass, Iwona Sobieraj, and Plumbley Mark D. A study of the complexity and accuracy of direction of arrival estimation methods based on gcc-phat for a pair of close microphones. In *Proceedings of the Detection and Classification of Acoustic Scenes and Events Workshop*, 2019.

Kaiming He, Xiangyu Zhang, Shaoqing Ren, and Sun Jian. Identity mappings in deep residual networks. In *European Conference on Computer Vision (ECCV)*, 2016a.

Yuhang He, Long Chen, and Jianda Chen. Multi-task relative attribute prediction by incorporating local context and global style information. In *Proceedings of the British Machine Vision Conference (BMVC)*, 2016b.

Yuhang He, Andrew Markham, and Niki Trigoni. Sounddet: Polyphonic sound event detection and localization from raw waveform. In *International Conference on Machine Learning (ICML)*, 2021.

Yedid Hoshen, Ron J. Weiss, and Kevin W. Wilson. Speech acoustic modeling from raw multichannel waveforms. In *2015 IEEE International Conference on Acoustics, Speech and Signal Processing (ICASSP)*, 2015.

Navdeep Jaitly and Geoffrey Hinton. Learning a better representation of speech soundwaves using restricted boltzmann machines. In *IEEE International Conference on Acoustics, Speech and Signal Processing (ICASSP)*, 2011.

Alex Kendall, Yarin Gal, and Roberto Cipolla. Multi-task learning using uncertainty to weigh losses for scene geometry and semantics. In *Computer Vision and Pattern Recognition (CVPR)*, 2018.

Diederik Kingma and Jimmy Ba. Adam: A method for stochastic optimization. In *3rd International Conference on Learning Representation (ICLR)*, 2015.

Tsung-Yi Lin, Michael Maire, Serge Belongie, James Hays, Pietro Perona, Deva Ramanan, Piotr Dollár, and C. Lawrence Zitnick. Microsoft coco: Common objects in context. In David Fleet, Tomas Pajdla, Bernt Schiele, and Tinne Tuytelaars (eds.), *European Conference on Computer Vision (ECCV)*, 2014.

Tsung-Yi Lin, Piotr Dollár, Ross Girshick, Kaiming He, Bharath Hariharan, and Serge Belongie. Feature pyramid networks for object detection. In *IEEE/CVF Conference on Computer Vision and Pattern Recognition (CVPR)*, 2016.

Wei Liu, Dragomir Anguelov, Dumitru Erhan, Christian Szegedy, Scott Reed, Cheng-Yang Fu, and Alexander Berg. Ssd: Single shot multibox detector. In *European Conference on Computer Vision (ECCV)*, 2016.

Ze Liu, Yutong Lin, Cao Yue, Han Hu, Yixuan Wei, Zheng Zhang, Stephen Lin, and Guo Baining. Swin transformer: Hierarchical vision transformer using shifted windows. In *IEEE/CVF Conference on Computer Vision and Pattern Recognition (CVPR)*, 2021.

Yi Luo and Nima Mesgarani. A sequence matching network for polyphonic sound event localization and detection. In *EEE/ACM Transactions on Audio, Speech and Language Processing*, 2019.

Stéphane Mallat. Group invariant scattering. In *Communications in Pure and Applied Mathematics*, 2012.

Ishan Misra, Abhinav Shrivastava, Abhinav Gupta, and Martial Hebert. Cross-stitch networks for multi-task learning. In *IEEE Conference on Computer Vision and Pattern Recognition (CVPR)*, 2016.

Satish Mohan, Michael Lockwood, Michael L. Kramer, and Douglas L. Jones. Localization of multiple acoustic sources with small arrays using a coherence test. In *The Journal of Acoustical Society of America*, 2008.

Mahesh Kumar Nandwana and T. Hasan. Towards smart-cars that can listen: Abnormal acoustic event detection on the road. In *Interspeech*, 2016.

Dimitri Palaz, Ronan Collobert, and Mathew Magimai-Doss. Estimating phoneme class conditional probabilities from raw speech signal using convolutional neural networks. In *Interspeech*, 2013.

Daniel Park, William Chan, Yu Zhang, Chung-Cheng Chiu, Barret Zoph, Ekin Cubuk, and Quoc V. Le. Specaugment: A simple data augmentation method for automatic speech recognition. 2019. URL https://arxiv.org/abs/1904.08779. arxiv:1904.08779.

Archontis Politis, Sharath Adavanne, and Tuomas Virtanen. A dataset of reverberant spatial sound scenes with moving sources for sound event localization and detection. In *Detection and Classification of Acoustic Scenes and Events Workshop (DCASE)*, 2020.

Mirco Ravanelli and Yoshua Bengio. Speaker recognition from raw waveform with sincnet. In *In IEEE Workshop on Spoken Language Technology (SLT)*, 2018.

Tara N. Sainath, Brian Kingsbury, Abdel-rahman Mohamed, and Bhuvana Ramabhadran. Learning filter banks within a deep neural network framework. In *IEEE Workshop on Automatic Speech Recognition and Understanding*, 2013.

Tara N. Sainath, Ron J. Weiss, Andrew Senior, Kevin W. Wilson, and Oriol Vinyals. Learning the speech front-end with raw waveform cldnns. In *Interspeech*, 2015.

Robin Scheibler, Eric Bezzam, and Dokmanić Ivan. Pyroomacoustics: A python package for audio room simulations and array processing algorithms. In *IEEE International Conference on Acoustics, Speech and Signal Processing (ICASSP)*, 2018.

Steffen Schneider, Alexei Baevski, Ronan Collobert, and Michael Auli. wav2vec: Unsupervised pre-training for speech recognition. In *Interspeech*, 2019.

Bob L Sturm. Stéphane mallat: A wavelet tour of signal processing, 2nd edition. *Computer music journal*, 2007.

Tho Nguyen Thi Ngoc, Ngoc Khanh Nguyen, Huy Phan, Lam Pham, Kenneth Ooi, Douglas Jones, and Woon-Seng Gan. A general network architecture for sound event localization and detection using transfer learning and recurrent neural network. In *IEEE International Conference on Acoustics, Speech, and Signal Processing (ICASSP)*, 2021.

T. N. Tho Nguyen, D. L. Jones, and W. Gan. A sequence matching network for polyphonic sound event localization and detection. In *IEEE International Conference on Acoustics, Speech and Signal Processing (ICASSP)*, 2020.

Sebastian Thrun. Affine structure from sound. In Y. Weiss, B. Schölkopf, and J. Platt (eds.), *Advances in Neural Information Processing Systems (NeurIPS)*, volume 18, pp. 1353–1360. MIT Press, 2006.

Ashish Vaswani, Noam Shazeer, Niki Parmar, Jacob Uszkoreit, Llion Jones Jone, Aidan N. Gomez, and Lukasz Kaiser. Attention is all you need. In *Advances in Neural Information Processing Systems (NeurIPS)*, 2017.

Qiang Wang, Li Zhang, Luca Bertinetto, Weiming Hu, and Philip H.S. Torr. Fast online object tracking and segmentation: A unifying approach. In *IEEE/CVF Conference on Computer Vision and Pattern Recognition (CVPR)*, 2019.

Qing Wang, Huaxin Wu, Zijun Jing, Feng Ma, Yi Fang, Yuxuan Wang, Tairan Chen, Jia Pan, Jun Du, and Chin-Hui Lee. The ustc-iflytek system for sound event localization and detection of dcase2020 challenge. In *Tech. Report of SELD Decase2020 Challenge*, 2020.

Bo Yang, Jianan Wang, Ronald Clark, Qingyong Hu, Sen Wang, Andrew Markham, and Niki Trigoni. Learning object bounding boxes for 3d instance segmentation on point clouds. In *Advances in Neural Information Processing Systems*, pp. 6737–6746, 2019.

Neil Zeghidour, Nicolas Usunier, Iasonas Kokkinos, Thomas Schatz, Gabriel Synnaeve, and Emmanuel Dupoux. Learning filterbanks from raw speech for phone recognition. In *IEEE International Conference on Acoustics, Speech and Signal Processing (ICASSP)*, 2018.

Neil Zeghidour, Olivier Teboul, Félix de Chaumont Quitry, and Marco Tagliasacchi. Leaf: A learnable frontend for audio classification. *International Conference on Learning Representations (ICLR)*, 2021.

A APPENDIX

A.1 SPATIAL LOCATION ENCODING IN FREQUENCY DOMAIN AND RECORDING FORMAT DISCUSSION

We discuss the detailed spatial location encoding for FOA and MIC sound waveform recording format. The spatial location encoding is based on 2D feature learned by the Gabor filter bank for each sound waveform channel, which can be represented as $\{F_i = (R_i, I_i)\}_{i=1}^{4}$. R_i and I_i are real part and imaginary part feature of the i-th channel sound waveform, respectively.

FOA format is well-known as first-order Ambisonics (B-format). It contains four channels: omni-directional, x-directional, y-directional and z-directional components, respectively. The instantaneous sound intensity vector is often used as spatial location (or phase difference) feature, which can be computed through the cross-spectrum between the omni-directional channel to the remaining x, y, z-directional. As a result, we have obtained 3 channel spatial location encoding feature.

$$IV_x = F_0^* \cdot F_1, \;\; IV_y = F_0^* \cdot F_2, \;\; IV_z = F_0^* \cdot F_3 \tag{6}$$

where F_0^* indicates the conjugate of the omni-directional feature. The three cross-spectrum feature IV_x, IV_y and IV_z are stacked together and further normalized before serving as the spatial encoding feature.

MIC format is well-known as tetrahedral microphone array. The four microphones are mounted in spherical coordinates with four distinct orientations. We treat the four microphones equally and compute the phase difference between any two microphones. Thus a total of six channels spatial location feature can be constructed. Specifically, we choose to compute GCC-PHAT(Brandstein & Silverman, 1997) like cross-spectrum feature. For any two channel m and n, we compute the angle between the real part and imaginary part of the cross-spectrum.

$$SL = angle(F_m^* \cdot F_n), \; m \neq n, m = 1, 2, 3, 4; n = 1, 2, 3, 4 \tag{7}$$

SL indicates the spatial location feature computed by the sound waveform channel m and n. The $angle(\cdot)$ equals to a frequency amplitude normalization operation, like the GCC-PHAT(Brandstein & Silverman, 1997) does. Please note that all the spatial location feature computation operations are differentiable so the whole neural network becomes end-to-end trainable.

A.2 NETWORK ARCHITECTURE AND TRAINING DETAILS

SoundSynp neural network architecture is given in Table 4. To train the neural network, we evenly divide the one minute long four-channel raw waveform into non-overlapping 4s short snippets. The raw waveform is first normalized to $[-1, 1]$ before feeding the neural network. We adopt Adam optimizer(Kingma & Ba, 2015) with an initial learning rate 0.0002 in the first 100 epochs and 0.00007 in the following 50 epochs. Batchsize is 16. The loss combination weight between classification head and regression head is $1 : 2$. During training, data augmentation method SpecAugment(Park et al., 2019) is applied. For DoA task, we regress direction of arrival angle in Cartesian coordinates $[x, y, z]$. In synperiodic filter bank groups, the filter length is 1025, each group's filter number is 256 and the step size is 600. Particularly, we have observed the initialized learnable synperiodic filter banks update its parameters intensively during the very early several epochs, and then gradually becomes stable. The final learned parameters are close to their initialization, one group's learned parameters (like frequency response and filter window length) is different from those learned by other groups, although they are initialized as the same in the start.

A.3 SYNPERIODIC FILTER BANK FREQUENCY-PERIODICITY RELATIONSHIP DETERMINATION

Mel-scale time-frequency representation has been widely used in both traditional sound feature like MFCC(Davis & Mermelstein, 1980), LogMel and learnable filter bank(Zeghidour et al., 2021). It initializes the filter bank in frequency domain, in which high-frequency filter has wider window length. We transform the filter bank into time domain and can naturally get a roughly logarithmic-scale frequency-periodicity relationship, in which narrower window width is associated with high-frequency

Table 4: SoundSynp neural network architecture. The layer follow $name@kernelsize, stride$ format, and synperiodic filter bank follow $name@kernelsize, stride, groups$ format. FC is fully connection layer, AvgPool is the average pooling layer, MaxPool is max-pooling layer. B is the batch-size, T is input waveform time-length. All convolution layers are followed by a batch normalization layer and Relu activation layer. We represent the neural network architecture on FOA recording format with sampling rate 24k Hz and label resolution 100 ms. It can be easily adjusted to fit other cases. Please note that since the backbone neural network has two identical branches, we just show one branch here.

layer	filter num	output size
Input: [B,4,T]		
Synperiodic Filter Bank Groups		
SynperiodicFilterBank@1024,600,3	256	[B, 256, T/600, 21]
Backbone Conv block1		
Conv2d@3,1	128	[B, 256, T/600, 128]
Conv2d@3,1	128	[B, 256, T/600, 128]
AvgPool@2,1	None	[B, 128, T/600, 128]
Backbone Conv block2		
Conv2d@3,1	256	[B, 128, T/600, 256]
Conv2d@3,1	256	[B, 128, T/600, 256]
AvgPool@2,1	None	[B, 64, T/600, 256]
Backbone Conv block3		
Conv2d@3,1	256	[B, 64, T/600, 256]
Conv2d@3,1	256	[B, 64, T/600, 256]
AvgPool@2,1	None	[B, 32, T/600, 256]
Backbone Conv block4		
Conv2d@3,1	512	[B, 32, T/600, 512]
Conv2d@3,1	512	[B, 32, T/600, 512]
AvgPool@2,1	None	[B, 16, T/600, 512]
Backbone Conv block5		
Conv2d@3,1	512	[B, 16, T/600, 512]
Conv2d@3,1	512	[B, 16, T/600, 512]
AvgPool@16,1	None	[B, T/600, 512]
Backbone MHSA block1		
MHSA@8,1024	512	[B, T/600, 512]
AvgPool@2,1	None	[B, T/1200, 512]
Backbone MHSA block2		
MHSA@8,1024	512	[B, T/1200, 512]
AvgPool@2,1	None	[B, T/2400, 512]
Backbone MHSA block3		
MHSA@8,1024	512	[B, T/2400, 512]
FC	class num	[B, T/2400, class num]
FC	class num x 3	[B, T/2400, class num x 3]
Trackwise Permutation Invariant Head		
Multi-label Classification	None	scalar
Location Regression	None	scalar

filters. We thus set $\omega(w_i, \rho) = 27 \cdot \log_{10}(w_i) - \rho$. We plot our synperiodic filter bank window function and the mel-scale initialized windowing function in Fig. 4, it shows our proposed windowing function naturally approximates the mel-scale windowing function.

A.4 Causality in Multi-scale frequency domain perception

Fig.5 shows how causality is achieved in multi-scale frequency domain perception.

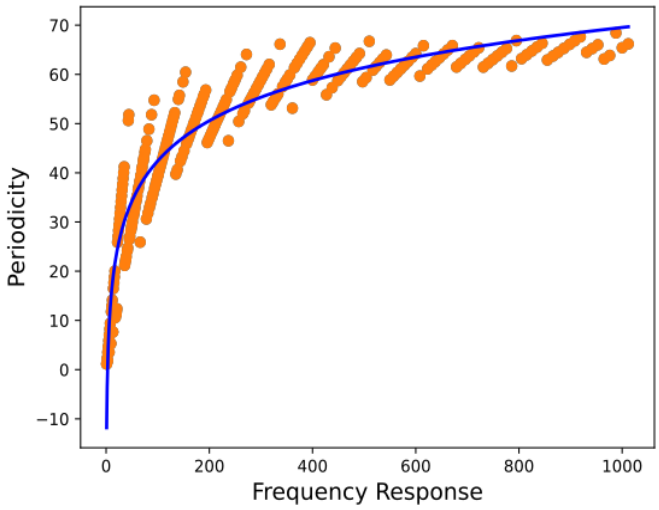

Figure 4: The relationship between filter frequency response and the periodicity. Green curve: our proposed windowing function. Light orange dots: mel-scale initialized frequency-periodicity relationship.

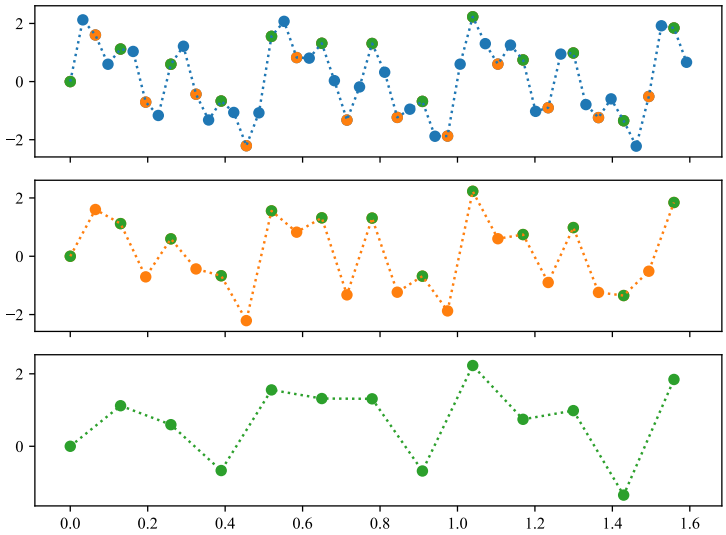

Figure 5: Consecutively downsampled waveform has longer time range in the original waveform (top row). So processing downsampled waveform increases the Causality.